A study of the electrical properties of HgS under high pressure

2007 J. Phys.: Condens. Matter 19 425222

(http://iopscience.iop.org/0953-8984/19/42/425222)

IOP PUBLISHING JOURNAL OF PHYSICS: CONDENSED MATTER

J. Phys.: Condens. Matter **19** (2007) 425222 (9pp) doi:10.1088/0953-8984/19/42/425222

A study of the electrical properties of HgS under high pressure

Aimin Hao[1,2], Chunxiao Gao[1,3,5], Ming Li[1], Chunyuan He[1], Xiaowei Huang[1], Dongmei Zhang[1], Cuiling Yu[1], Hongwu Liu[1], Yanzhang Ma[3], Yongjun Tian[4] and Guangtian Zou[1]

[1] State Key Laboratory for Superhard Materials, Institute of Atomic and Molecular Physics, Jilin University, Changchun 130012, People's Republic of China
[2] Department of Mathematics and Physics, Hebei Normal University of Science and Technology, Qinhuangdao 066004, People's Republic of China
[3] Department of Mechanical Engineering, Texas Tech University, Lubbock, TX 79409, USA
[4] State Key Laboratory for Metastable Materials Science and Technology, College of Materials Science and Engineering, Yanshan University, Qinhuangdao 066004, People's Republic of China

E-mail: cxgao599@yahoo.com.cn

Received 3 August 2007
Published 18 September 2007
Online at stacks.iop.org/JPhysCM/19/425222

Abstract

Using a microcircuit fabricated in a diamond anvil cell, we carried out *in situ* conductivity measurements on α-HgS and β-HgS under high pressure, and investigated the temperature dependence of the conductivity of the samples under several pressures. For α-HgS, the results show that the conductivity increases rapidly with increasing pressure from 8 to 20 GPa. The energy gap was obtained by fitting linearly the plot of the logarithm of conductivity versus the reciprocal of temperature. At 29 GPa, the sample becomes metallic, characterized by a negative temperature slope of conductivity and a zero energy gap. For β-HgS, a discontinuity of conductivity was observed at 5 GPa, corresponding to a transition from the β phase to the α phase. From 5 to 20 GPa, the conductivity rises rapidly with increasing pressure. At 27 GPa, the sample becomes metallic. In comparison with HgSe and HgTe, we obtained experimentally the transition pressure of the two samples from the cinnabar structure to the rock-salt structure, respectively.

(Some figures in this article are in colour only in the electronic version)

1. Introduction

The mercury chalcogenides exhibit structural and electronic properties somewhat different from the other members of the group. According to the ionicity defined by Philips and Van Vechten [1], HgS has an ionicity of 0.79, which is the borderline between the ionic rock-salt structure and the covalent zincblende structure of $A^N B^{8-N}$ compounds.

[5] Author to whom any correspondence should be addressed.

There are two different structures of HgS under ambient conditions. One is cinnabar (α-HgS), which has a hexagonal structure (space group $P3_121$) and a red color. The other (β-HgS) has a zincblende (metastable) structure (space group $F43m$) and a black color.

The general question as to whether or not a material is a metal is of basic importance, since the existence of a fundamental energy gap will affect a material's properties in a profound way. Under ambient conditions, α-HgS is a direct band gap semiconductor with a wide energy gap of 2.1 eV [2] from Γ_V to Γ_C [3]. It becomes an indirect band gap semiconductor from A_V to M_C at pressures higher than 8 GPa [3].

Recently, however, whether or not β-HgS is a semimetal has been a subject of controversy, with the band gap being reported to be both negative and positive [4–7]. For example, a theoretical calculation based on density function theory (DFT) found that β-HgS has a small spin–orbit-induced band gap [4]. The Shubnikov–de Haas effect showed that the negative energy gap is close to -0.190 eV [5]. Optical measurement provided evidence that β-HgS has an inverted band structure, with an energy gap of -0.15 eV [6]. With calculations based on density functional theory within the local density approximation (LDA), Delin found that β-HgS has at the same time an inverted band structure and a small fundamental energy gap, and suggested that β-HgS is actually a semiconductor, not a semimetal [7].

Under very high pressure, a relatively open structure may eventually collapse and transform to another structure. So the local structure of tetrahedrally bonded compounds is destabilized, and evolves toward a six-fold coordination geometry. Bridgeman tried to study the compression of β-HgS without success, because the black HgS turned into the red form when he precompressed it to 5 GPa [8]. Huang *et al* studied the high-pressure transition of α-HgS by energy dispersive x-ray diffraction using a synchrotron x-ray source and found that the cinnabar structure transforms to rock-salt (RS) structure at about 13 GPa [9]. However, the high-pressure x-ray and high-pressure Raman studies showed no evidence of any phase transitions up to 22 GPa [10]. Huang *et al*, again, reported that a diffraction pattern obtained at 30 GPa has been indexed as an RS-structure with a reliability factor of $R = 0.16$ ($R = 0$ represents a perfect fit) [11]. Recently, Sun *et al* studied the pressure-induced phase transition of α-HgS by first-principle computation and found that α-HgS transforms to RS–HgS at a pressure of 26.57 GPa [12].

As stated above, the transition pressure from the α-phase to the RS-phase is still an open question. So it is necessary to reinvestigate it experimentally. In addition, the pressure applied in the above resistivity (or conductivity) measurement was limited to about 20 GPa. Above 20 GPa, the electrical properties of HgS have hitherto been unexplored. So it is expected that a further measurement of the electrical property will be undertaken at a more elevated pressure.

The conductivity (or resistivity) is an important property of materials under high pressures, which may imply the phase transitions or some clues of the changes in the electronic configuration. Since the early work of Drickamer *et al* [13, 14] on the resistance discontinuity of IIB–VI and III–V compounds as a function of pressure, many works have been made to identify the crystal–structural transitions corresponding to these resistance changes [15–18]. In the present work, we investigated the conductivity of α- and β-HgS under high pressure to obtain information about the phase transition. The temperature dependence of conductivity was also studied to obtain information about the energy gap, and to identify experimentally whether β-HgS is a semimetal.

2. Experimental details

In the present work, we used a Mao-Bell type diamond anvil cell (DAC) and T301 stainless steel as the gasket. The pressure was determined using the ruby fluorescence method. The

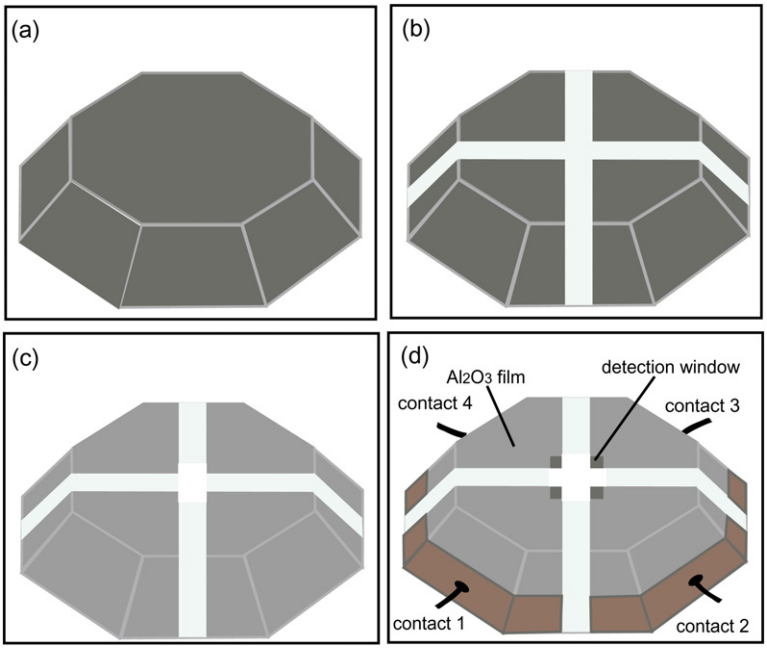

Figure 1. Manufacturing process and configuration of a microcircuit in a diamond anvil.

samples, α- and β-HgS with a purity of 99.999% (purchased from Alfa Aesar Company), were ground into fine powder with an average size of 5 μm for uniformity of experimental conditions between runs.

Molybdenum and alumina were chosen as electrode and insulation materials, respectively. The selection was based on the following considerations. First, both molybdenum and alumina have a large modulus (Mo $\sim$ 230 GPa, Al_2O_3 $\sim$ 240 GPa), so they can strongly resist plastic flow under high pressure. Second, molybdenum and alumina have no pressure-induced phase transition up to 210 GPa [19] and 175 GPa [20], respectively. Finally, Al_2O_3 has high hardness (HB $\sim$ 1500 kgf mm^{-2}), good wearability, and can remain to be an insulator under high pressure [21].

A radio frequency (rf) magnetron sputtering system was used to deposit an Mo film of 300 nm onto a diamond anvil, as shown in figure 1(a). Then, the Mo film was chemically patterned into the configuration of a van der Pauw four-probe microcircuit, as shown in figure 1(b). These sections were used as current- and voltage-ends, respectively. The microcircuit and diamond culet were then encapsulated with 2 μm-thick alumina as the insulation layer, as shown in figure 1(c). In order to make the four electrodes contact the sample, selected areas of alumina were removed chemically to form a detection window with a size of 120 μm $\times$ 120 μm, as shown in figure 1(d). For fabrication details, see references [22–25]. The diagram of a microcircuit and a sample arranged in a DAC is shown in figure 2.

The van der Pauw method with the following formula was utilized to calculate the conductivity of the sample:

$$\exp(-\pi l R_A \sigma) + \exp(-\pi l R_B \sigma) = 1, \tag{1}$$

where σ and l are the conductivity and the thickness of the sample, respectively; and R_A and R_B are electrical resistances with $R_A = V_{43}/I_{12}$ and $R_B = V_{14}/I_{23}$, respectively. In the

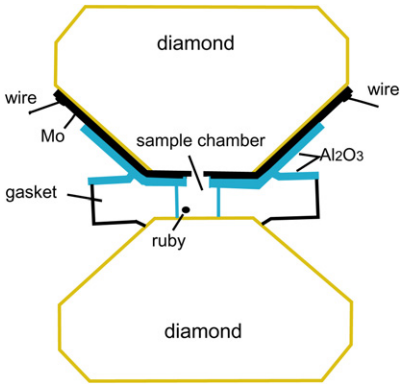

Figure 2. Diagram of a microcircuit and a sample arranged in a DAC under its working condition.

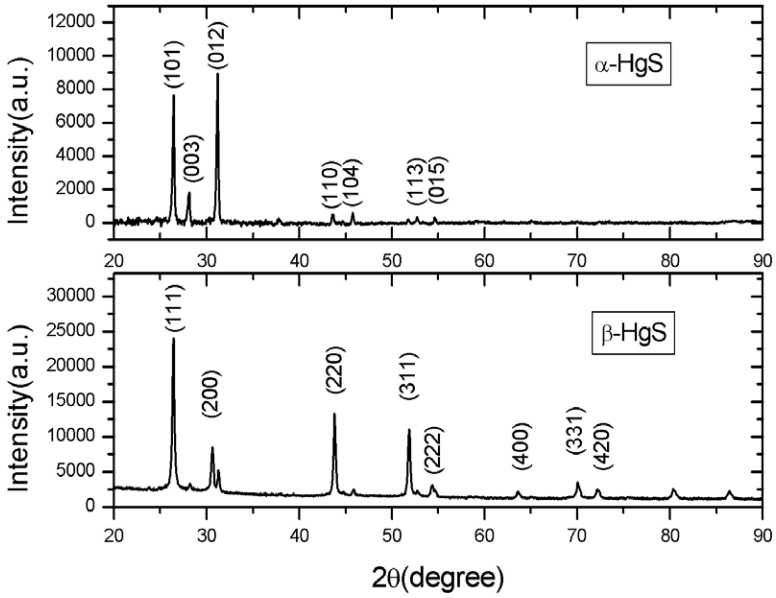

Figure 3. The x-ray diffraction patterns on the two samples at ambient conditions.

measurement, a current I_{12} was applied across the contacts 1 and 2, and the potential difference V_{43} across the contacts 3 and 4 was measured with a precise multimeter (Hewlett-Packard, 3458A); similarly, a current I_{23} was applied across the contacts 2 and 3, and the potential difference V_{14} across the contacts 1 and 4 was measured. The thickness of the sample was measured at every pressure.

3. Results and discussions

The x-ray diffraction patterns on the two samples are shown in figure 3. The structure of the red powder at ambient conditions was determined to be the cinnabar structure with lattice

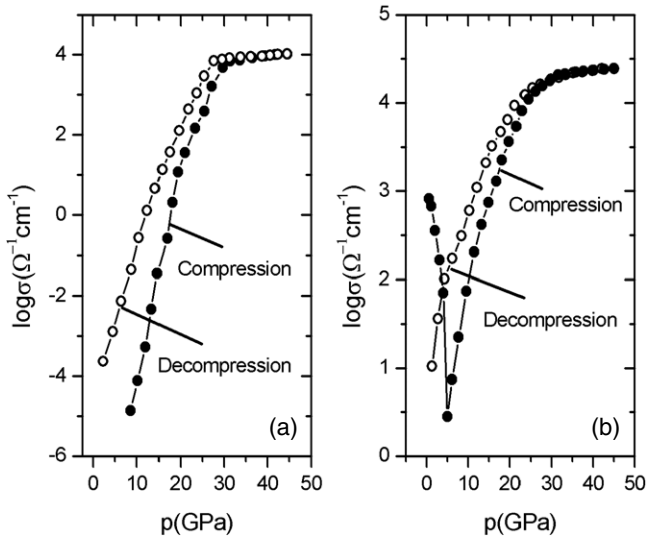

Figure 4. The plots of $\log\sigma$ versus p of the two samples at room temperature. (a) α-HgS, (b) β-HgS, initially.

parameters $a = b = 4.145$ Å and $c = 9.496$ Å, while the black powder at ambient conditions was determined to be the zincblende structure with lattice parameters $a = b = c = 5.846$ Å.

3.1. The conductivity measurement of the two samples under high pressure

We carried out *in situ* conductivity measurements on the two samples under high pressure and at room temperature. The results are shown in figure 4.

For the first sample, below 8 GPa, the resistance of the sample is so huge that the electric current was unable to be detected. Above 8 GPa, the conductivity increases rapidly with increasing pressure. From 20 to 29 GPa, the conductivity increases gradually with increasing pressure. At 29 GPa, the conductivity reaches the order of $10^4\ \Omega^{-1}\ \mathrm{cm}^{-1}$. During decompression, a similar change in conductivity was observed with some hysteresis.

For the second sample, the conductivity decreases rapidly with increasing pressure by a factor of 10^3 from ambient pressure to 5 GPa. Corresponding to the phase transition from β phase to α phase, a discontinuity in conductivity was observed at 5 GPa. A possible reason for the discontinuity in conductivity may be due to the change in the density of electronic states at the structural transition. Also, it was observed that the black sample turned red gradually, starting at 5 GPa, with a subsequent sharp increase in conductivity with increasing pressure, and reached a plateau of more than $10^4\ \Omega^{-1}\ \mathrm{cm}^{-1}$ at 27–46 GPa.

Upon decompression, the color of the sample stayed red to ambient pressure without turning back into black, and the conductivity did not return in its original magnitude either. Perhaps the β-to-α phase transition was irreversible, or it was reversible but too sluggish to be detected by the conductivity measurement.

As a comparison, the resistivity of HgTe was measured as a function of pressure with a four-probe method, and the resistivity increased by a factor of greater than 10^4 accompanying the phase transition from an ambient-pressure phase [26] to the cinnabar phase at 1.6 GPa [27]. The resistivity of HgSe increased by three orders of magnitude when the zincblende phase transforms to the cinnabar structure at 1 GPa [28].

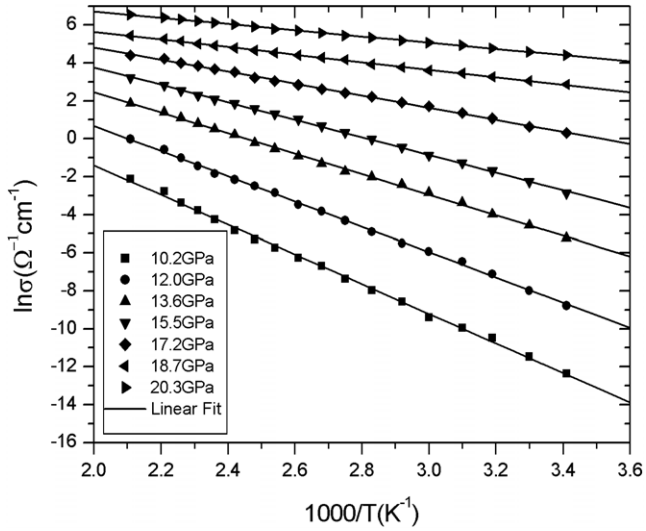

Figure 5. The plots of $\ln\sigma$ versus $1000/T$ for the first sample at several pressures.

3.2. The measurement of the energy gap of the two samples

We measured the temperature dependence of conductivity of the two samples at several pressures. For the first one, the result is shown in figure 5; for the second one, the case is similar.

In the intrinsic region, the relationship between the conductivity, the energy gap and the temperature of a semiconductor can be represented by the following equation [29–31]:

$$\sigma = \sigma_0 \exp(-E_g/2k_B T), \tag{2}$$

where σ_0 is a constant, which depends partially upon the electron and hole effective masses; k_B is the Boltzmann constant; T is the temperature; and E_g is the energy gap.

According to equation (2), the relationship between E_g and the slope of $\ln\sigma$ versus $1/T$ can be expressed as

$$E_g = -k_B[\partial \ln\sigma/\partial(1/T)]. \tag{3}$$

The energy gaps were obtained by fitting linearly the plots of $\ln\sigma$ versus $1000/T$, as shown in figure 6.

Similarly, we measured the temperature dependence of conductivity of the second sample, and obtained the plot of the energy gap versus pressure, as shown in figure 6.

For the first sample, the energy gap becomes zero at 29 GPa, which is a sign of metallization. The transition pressure is consistent with that of first-principle computation [12]. For the second sample, the energy gap becomes zero at 27 GPa.

The decrease in the energy gap with pressure is explained by a fundamental property of semiconductors, which is attributed to band widening by strengthened overlap interaction of the wavefunction with shrinking atomic distance [32].

The plots of E_g versus p in figure 5 were fitted to a quadratic function [29, 31],

$$E_g = E_{g0} + \alpha p + \beta p^2, \tag{4}$$

where E_{g0} is a constant; α and β are the first-order and second-order pressure derivatives, respectively. The fitted result is tabulated in table 1.

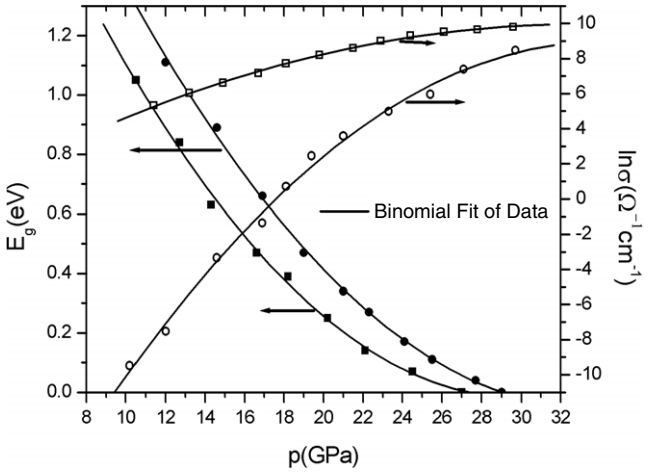

Figure 6. The plots of E_g versus p and the plots of $\ln\sigma$ versus p for the two samples. The symbols ● and ○ show E_g and $\ln\sigma$ of the first sample at pressure, respectively; the symbols ■ and □ show E_g and $\ln\sigma$ of the second sample at pressure, respectively.

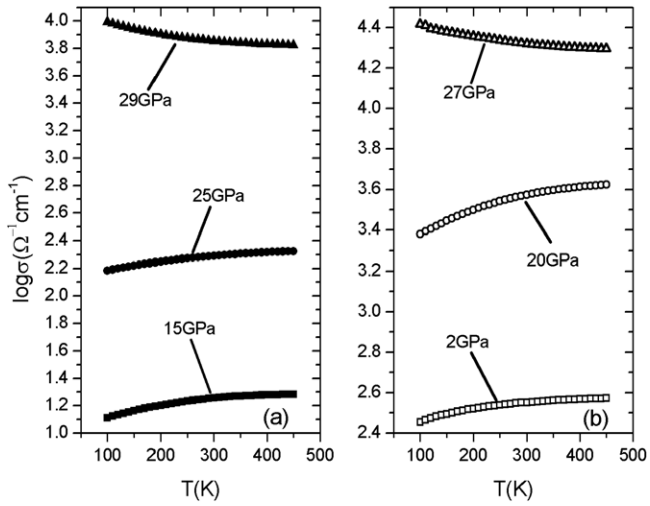

Figure 7. The plots of the conductivity versus temperature of the two samples: (a) the plots are for the first sample, which is initially α-HgS; (b) the plots are for the second sample, which is initially β-HgS.

Table 1. The parameter comparison for the two samples. p_m is the metallization pressure.

Parameters	α (eV GPa^{-1})	β (eV GPa^{-2})	E_{g0} (eV)	p_m (GPa)
The first sample	0.17	2.5×10^{-3}	2.81	29
The second sample	0.17	2.9×10^{-3}	2.53	27

3.3. The temperature dependence of conductivity of the two samples

We carried out measurements of the temperature dependence of conductivity at several pressures on the samples, as shown in figure 7.

For the first sample, at $p = 15$ and 25 GPa, $d\sigma/dT > 0$, which indicates the electrical property of a semiconductor. At $p = 29$ GPa, $d\sigma/dT < 0$, which indicates the electrical property of a conductor. Evidently, HgS becomes metallic at this pressure. According to [3], the top valence bands are composed of the combination of Hg-d and S-p states, and the lowest conduction bands consist of combination states of Hg-s and S-p and a little of Hg-d. The isotropy of the valence electron distribution is enhanced during the phase transition from cinnabar to rock-salt.

For the second sample, at $p = 2$ GPa, $d\sigma/dT > 0$. According to the order of magnitude of conductivity and the positive temperature slope of the conductivity, we thought β-HgS is a semimetal. At $p = 20$ GPa, $d\sigma/dT > 0$, which indicates the electrical property of a semiconductor. At $p = 27$ GPa, $d\sigma/dT < 0$, which indicates the sample becomes metallic at this pressure.

As a comparison, HgTe and HgSe become metallic at 8.4 GPa and 15.5 GPa, respectively [33]. Also, both HgTe and HgSe transform from the cinnabar structure to the NaCl structure as they become metallic [34, 35].

For ZnS, ZnSe and ZnTe, the zincblende structure becomes unstable and transforms into the NaCl structure, which is metallic in nature, at 14.7 GPa, 13.0 GPa and 9.5 GPa, respectively [36, 17]. So it is worth noting that the metallization pressure decreases with an increasing atomic number of the anion for the zinc chalcogenides. According to our result and reference [34], so does the metallization pressure for the mercury chalcogenides. The reason may be due to a consequence of having a larger number of core electrons, so that the effective potential for the valence and conduction electrons becomes weaker, because of the cancellation between the crystal potential and the repulsive potential produced by orthogonalization to the core states [37, 38]. This leads to the fact that the ionization energy of the conduction electrons for the heavier atom in the same group of the periodic table is smaller.

4. Conclusions

In summary, we have measured the *in situ* conductivity of α-HgS and β-HgS under high pressures and investigated the temperature dependence of conductivity of the samples under several pressures using a microcircuit fabricated on a DAC. For α-HgS, the result shows that the conductivity increases rapidly with increasing pressure, indicating the electrical property of a semiconductor. From 20 to 29 GPa, the conductivity increases gradually with increasing pressure. The energy gap was obtained by fitting linearly the plot of $\ln\sigma$ versus $1/T$. The sample becomes metallic at 29 GPa, corresponding to a transition from the cinnabar structure to the rock-salt structure. This result is consistent with that of the first-principles computation. For β-HgS, the result shows that the conductivity decreases rapidly with increasing pressure by three orders of magnitude from ambient pressure to 5 GPa. A discontinuity of conductivity evidently occurs at 5 GPa, corresponding to the transition from β-HgS to α-HgS. The sample becomes metallic at 27 GPa, corresponding to the transition from the cinnabar structure to the rock-salt structure. In addition, our experimental results show that β-HgS is a semimetal.

Acknowledgments

This work was supported by the National Natural Science Foundation of China (grant nos. 40473034, 10574055, and 50532020), and the National Basic Research Program of China (grant no. 2005CB724404).

References

[1] Philips J C and Van Vechten A J 1970 *Phys. Rev.* B **2** 2147
[2] Roberts G G and Zallen R 1971 *J. Phys. C: Solid State Phys.* **4** 1890
[3] Sun S R, Li Y C, Liu J, Dong Y H and Gao C X 2006 *Phys. Rev.* B **73** 113201
[4] Delin A and Klüner T 2002 *Phys. Rev.* B **66** 035117
[5] Dybko K, Szuszkiewicz W, Dynowska E, Paszkowicz W and Witkowska B 1998 *Physica* B **258** 629
[6] Zallen R and Slade M 1970 *Solid State Commun.* **8** 1291
[7] Delin A 2002 *Phys. Rev.* B **65** 153205
[8] Bridgman P S 1940 *Proc. Am. Acad. Arts. Sci.* **74** 21
[9] Huang T and Ruoff A L 1983 *J. Appl. Phys.* **54** 5459
[10] Werner A, Hochheimer H D and Strössner K 1983 *Phys. Rev.* B **28** 3330
[11] Huang T and Ruoff A L 1985 *Phys. Rev.* B **31** 5976
[12] Sun S R and Dong Y H 2005 *Phys. Rev.* B **72** 174101
[13] Minomura S and Drickamer H G 1962 *J. Phys. Chem. Solids* **23** 451
[14] Samara G A and Drickamer H G 1962 *J. Phys. Chem. Solids* **23** 457
[15] Owen N B, Smith P L, Martin J E and Wright A J 1963 *J. Phys. Chem. Solids* **24** 1519
[16] Smith P L and Martin J E 1964 *Phys. Lett.* **19** 541
[17] Ohtani A, Motobayashi M and Onodera A 1980 *Phys. Lett.* A **75** 435
[18] Kasper J S and Brandhorst M 1964 *J. Chem. Phys.* **41** 3768
[19] Hixson R S, Boness D A, Shaner J W and Moriarty J A 1989 *Phys. Rev. Lett.* **62** 637
[20] Japhcoat R S, Hemley R J and Mao H K 1988 *Physica* B **150** 115
[21] Grzybowski T A and Ruoff A L 1984 *Phys. Rev. Lett.* **53** 489
[22] Han Y H, Gao C X, Ma Y Z, Liu H W, Pan Y W, Luo J F, Li M, He C Y, Huang X W and Zou G T 2005 *Appl. Phys. Lett.* **86** 064104
[23] Han Y H, Luo J F, Hao A M, Gao C X, Xie H S, Qu S C, Liu H W and Zou G T 2005 *Chin. Phys. Lett.* **22** 927
[24] Gao C X, Han Y H, Ma Y Z, White A, Liu H W, Luo J F, Li M, He C Y, Hao A M, Huang X W, Pan Y W and Zou G T 2005 *Rev. Sci. Instrum.* **76** 083912
[25] Hao A M, Gao C X, Li M, He C Y, Huang X W, Zhang D M, Yu C L, Zou G T, Li Y C, Li X D and Liu J 2006 *Chin. Phys. Lett.* **23** 2917
[26] Mariano A N and Warekois E P 1963 *Science* **142** 672
[27] Blair J and Smith A C 1961 *Phys. Rev. Lett.* **7** 124
[28] Ramesh T G and Shubha V 1982 *J. Phys. C: Solid State Phys.* **15** 6193
[29] Anthony L C and Peter Y Y 1993 *Phys. Rev. Lett.* **71** 4011
[30] Kobayashi H, Takeshita N, Môri N, Takahashi H and Kamimura T 2001 *Phys. Rev.* B **63** 115203
[31] DiMarzio D, Croft M and Sakai N 1987 *Phys. Rev.* B **35** 8891
[32] Paul W and Warschauer D M 1963 *Solids Under Pressure* ed W Paul and D M Warschauer (New York: McGraw-Hill) p 179
[33] Ohtani A, Seike T, Motobayashi M and Onodera A 1982 *J. Phys. Chem. Solids* **43** 627
[34] Lu Z W, Singh D and Krakauer H 1989 *Phys. Rev.* B **39** 10154
[35] Huang T and Ruoff A L 1983 *Phys. Rev.* B **27** 7811
[36] Karzel H, Potzel W and Köfferlein M 1996 *Phys. Rev.* B **53** 11425
[37] Cohen M N and Heine V 1961 *Phys. Rev.* **122** 1821
[38] Philips J C and Kleinman L 1959 *Phys. Rev.* **116** 287